Deutscher Luft- und Raumfahrtkongress 2008
DocumentID: 81319

THE GEOFLOW-EXPERIMENT ON ISS: IMAGE PROCESSING AND FLOW ANALYSIS

S. Koch, N. Dahley, B. Futterer, T. von Larcher, N. Scurtu, L. Jehring C. Egbers

Dept. Aerodynamics and Fluid Mechanics
Brandenburg University of Technology Cottbus, Siemens-Halske-Ring 14, 03046 Cottbus, Germany
E–Mail: sandy.koch@tu-cottbus.de - Homepage: http://www.tu-cottbus.de/LAS

Abstract

The research of thermal convection in spherical shells under the influence of a radial force field is a fundamental model in geophysical fluid dynamics. The European microgravity experiment GeoFlow, which is executed in the Fluid Science Laboratory (FSL) in the Columbus module on the International Space Station (ISS), is an experiment for investigating pattern formation and stability of thermal convection in rotating spherical shells under influence of a central symmetry buoyancy field. The flow visualization is realized with the Wollaston-Shearing-method.
The focus in this paper is on the numerical preliminary studies of this spherical Rayleigh-Bénard problem under a central dielectrophoretic force in microgravity environment. Numerical simulations are done with a pseudospectral method and are accomplished for a range of parameter values for Rayleigh and Taylor number. In addition, we describe the way of image processing and the analysis of the experimental data.

1 Introduction

The microgravity experiment GeoFlow is an European project, integrated in the Fluid Science Laboratory (FSL) in the Columbus module on the International Space Station (ISS). This experiment focus on the research of stability and pattern formation of thermal convection in a rotating spherical gap with an artificial central dielectrophoretic force field by applying a high voltage alternating field on the inner sphere [6], [11] and [1].

For a preparation for the execution of the experiment on the ISS there were carried out lot of preliminary investigations on the Engineering Model (EM) from the industry partner and at the Science Reference Model (SRM) at BTU Cottbus. Comparative to the experimental tests, a rich variety of numerical simulations were computed ([7] and [9]). These numerical studies are used for preparation of the experimental design and complementary parameter variations as well as analysis of both, stable and time-dependent flows, that was found to exist in the parameter range of the GeoFlow experiment. The problem of convection in spherical shells has been considered before in various research programs. Critical Rayleigh numbers were calculated by Joseph and Carmi [4], via linear and energy stability analysis in the non-rotating case for different central force fields. Roberts [12] calculated the flow and critical Rayleigh numbers in the limit of very rapid rotation, and found that the critical Rayleigh numbers depends on the Taylor number according to $Ra_c \sim Ta^{2/3}$. Busse [3] has also considered that case, and predict that the flow should take the form of "columnar cells". Hart et al. [8] considered this problem, too, using a hemispherical shell model and neglecting the centrifugal force.

Here, we present results of numerical simulations and this results for a) non-rotating cases, b)roting cases in reference to the experiment. In addition, the data analysis of the wollaston-shearing interferograms is described. The processed interferograms are used for the calculation of the temperature field.

By comparing numerical and experimental results, it should be possible to determine the dynamic of the observed flow patterns.

2 Numerical Simulations

The non-dimensional equations for thermal convection in rotating spherical shells under influence of the dielectrophoretic force field regard the velocity field $\mathbf{U}$ and temperature field T by

(1) $$\nabla \cdot \mathbf{U} = 0,$$

(2)
$$Pr^{-1}\left[\frac{\partial \mathbf{U}}{\partial t} + (\mathbf{U}\cdot\nabla)\mathbf{U}\right] = -\nabla p + \nabla^2 \mathbf{U} + Ra\, T\, \hat{\mathbf{e}}_z + Ra_{central}\, T\, \hat{\mathbf{e}}_r + \sqrt{Ta}\,\hat{\mathbf{e}}_z \times \mathbf{U} + \widetilde{Ra}\, T\, r \sin\theta \hat{\mathbf{e}}_{eq}$$

(3) $$\frac{\partial T}{\partial t} + (\mathbf{U}\cdot\nabla)T = \nabla^2 T.$$

Refer also to [2] for a detailed description of scaling the equational system and evolution of parameters. Then the GeoFlow experiment is described with the Prandtl number

(4) $$Pr = \frac{\nu}{\kappa}$$

as a material property of the fluid (ν and κ are the fluid's viscosity and thermal diffusivity, respectively), and the Rayleigh number for measuring the imposed thermal forcing. Natural convection in spherical gaps with $d = r_o - r_i$, in an axial force field in an earth laboratory, is described by

(5) $$Ra = \frac{\alpha \Delta T g d^3}{\nu \kappa}$$

with α as the thermal expansion coefficient, factor g is acceleration due to gravity. For the dielectrophoretic force field set-up the parameter $Ra_{central}$ describes the central buoyancy thermal convection

(6) $$Ra_{central} = \frac{\gamma \Delta T g_e d^3}{\nu \kappa}.$$

Here γ is the dielectric variability and g_e the electric acceleration due to electrohydrodynamic force, variable in strength by V_{rms}, which is the high voltage alternating electrical field giving the central force. Regarding convection in earth laboratory, superimposed with high voltage field, both Rayleigh numbers have to be considered. For the microgravity environment at ISS only $Ra_{central}$ is necessary.

The system is rotating with constant rotational frequency $N = \Omega/(2\Pi)$. Those effects are treated in Coriolis and centrifugal forces, described by Taylor number

(7) $$Ta = \left(\frac{2\Omega d^2}{\nu}\right)^2$$

and the additional factor

(8) $$\widetilde{Ra} = \frac{\alpha \Delta T}{4}\, Pr\, Ta.$$

The boundary conditions associated with (Eq. 2) are no-slip for velocity field $\mathbf{U}$ and for temperature equation (Eq. 3) they correspond to inner heating and outer cooling of spherical shells.

This system of equations and boundary conditions is solved using the numerical code of [9], in which $\mathbf{U}$ and T are expanded in terms of Chebyshev polynomials in radial direction r, and Legendre functions in meridional θ and azimuthal direction φ. For numerical simulation the parameter $Ra_{central}$ has to be used without geometry. In the following the denoted Rayleigh number is defined as $Ra_{central} = (2\,\epsilon_r\,\epsilon_r\,\gamma)/(\rho\,\nu\,\kappa)\cdot\Delta T V_{rms}^2$, showing also that for the final experiment temperature difference ΔT and high voltage V_{rms} are the parameters which give the drive for convection.

Further values for the calculations come along with experimental constraints. So working fluid, filling the spherical gap, is a silicone oil of GE Bayer Silicones, having a Prandtl number $Pr = 64.64$. With the inner radius $r_i = 27\ mm$ and outer radius $r_o = 54\ mm$ the radius ratio gets $\eta = 0.5$. Experimental runs are composed of applying a constant voltage $V_{rms} = 10\ kV$ and varying ΔT up to $10\ K$, the Rayleigh number than reaches $Ra_{central} \leq 1.4 \cdot 10^5$. A possible rotation rate up to $2\ Hz$ results in Taylor number $Ta_{max} = 1.3 \cdot 10^7$.

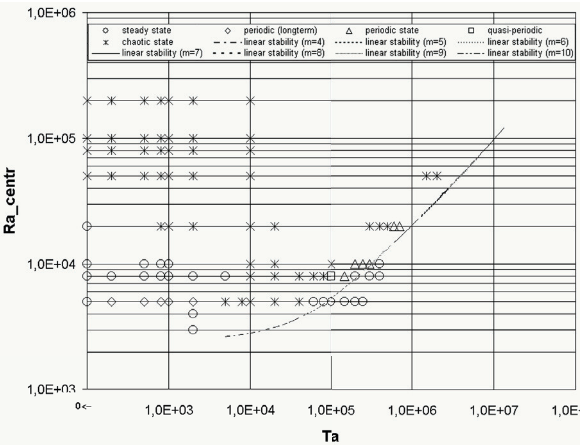

Figure 1: Overview of convective states in spherical shells of $\eta = 0.5$ for $Pr = 64.64$ depending on $Ra_{central}$ and Ta: Besides time-dependency of numerical solution diagram show linear stability of most unstable modes m.

2.1 Results for Thermal Convection in Different Rotating Regimes

Main parts of parameter variation include set-up of temperature gradient between inner and outer sphere (corresponding to Rayleigh number variation) and rotation of spherical system (corresp. to Taylor number variation). Figure 1 shows this parameter regime and calculated convective states. Experiment runs follow this diagram with a non-rotating case, where Rayleigh number is increased stepwise, and rotating cases, where a distinct temperature difference is set-up (Ra fixed) and then rotation rates are superimposed by increasing Ta, starting with low rotation regime to intermediate to high rotation regime. In the following these different regions are discribed.

2.1.1 Non-Rotating Case

Increasing Rayleigh number corresponds to strength thermal impulse of the system. Transition from basic state to steady and then direct to irregular time-dependent convective states are found (Fig. 1). Patterns of steady state convection depend on initial state. Increasing stepwise leads

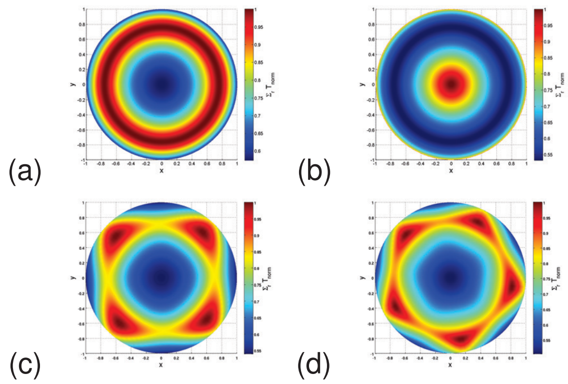

Figure 2: Patterns of convective steady states for non-rotating case $Ta = 0$: (a) - axisymmetry at $Ra_{central} = 5000$, (b) - inverse axisymmetry at $Ra_{central} = 8000$, (c) - cubic symmetry at $Ra_{central} = 5000$, (d) - symmetry with azimuthal wave number 5 at $Ra_{central} = 10000$. Pictures show summed radial temperature at northern hermisphere.

to axisymmetric states (Fig. 2 a-b), setting thermal impulse immediatly from zero reveals complex symmetries (Fig. 2 c-d). With methods of path following stability of patterns are validated in those different ranges. For experimental work on ISS different patterns will be observable due to different runs with changing the initial states. Refer also to [7] and [2] for more details on stability discussions. For irregular flow tetrahedral patterns dominate flow structures.

2.1.2 Rotating Case

From low to intermediate to high rotation the experiment travers stability lines of most unstable modes (Fig. 1). The higher the rotation, the higher the azimuthal mode of convective flow (Fig. 3). Furthermore a change of drift velocity occurs, predicted also with stability analysis from [13]. Direct numerical simulation results show prograde drift for low rotation regime and retrograde drift for intermediate rotation regime. For low rotation patterns are just rotated but not distorted. For intermediate rotation patterns start to align at tangent cylinder. Centrifugal effects come into account.

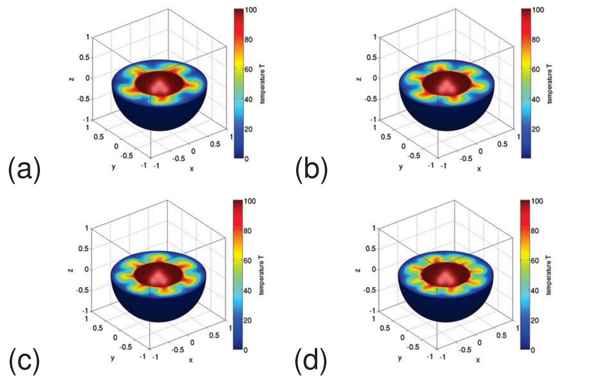

Figure 3: Patterns of convective steady states for rotating case $Ta \neq 0$: (a) - $m = 5$ at $Ta = 1 \cdot 10^5$, $Ra_{central} = 8000$, (b) - $m = 6$ at $Ta = 2 \cdot 10^5$, $Ra_{central} = 10000$, (c) - $m = 7$ at $Ta = 6 \cdot 10^5$, $Ra_{central} = 2000$, (d) - $m = 8$ at $Ta = 1.5 \cdot 10^6$, $Ra_{central} = 50000$. Pictures show radial temperature field in meridional cut.

Calculations for high rotation are not finished yet. Additionally time-series analysis for complex time dependency behaviour is necessary. Final goal is to track the transition from basic via steady to periodic and chaotic state for fixed Ta and increasing Ra as marked in diagram of Figure 1.

3 Data analysis

Figure 4 shows the way of the data processing, evaluation and data interpretation. On the left side, the forward modelling with the simulation of the 3D temperature field which is used for construction of numerical interferograms is demonstrated. This allows the comparison with the experimental interferograms. On the right side, the inverse modeling with calculation of the integrated temperature field which is based on experimental data, is shown. An example to demonstrate the inverse modelling and to illustrate the forward modelling is given in the next section. This allows the comparison with numerical calculated temperature fields. The observed flow pattern can be analysed in detail by using this data flow in a useful manner and that allows a characterization of the flow pattern. Also the numerical simulations can be verified with experimental data.

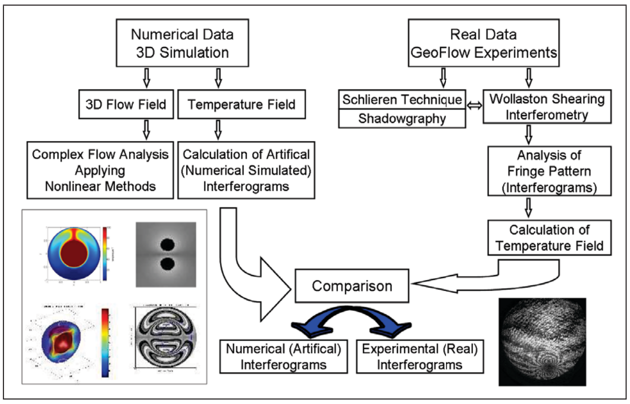

Figure 4: Numerical and experimental data analysis. Verification of experimental data by analysis and comparison with numerical data.

3.1 Image Processing

The temperature field $T(\vartheta, \phi)$:

$$T(\vartheta, \phi) = \frac{\Delta\vartheta\ \lambda}{2\ d\ \varepsilon} \cdot \left(\frac{dn}{dT}\right)^{-1} \int_{\vartheta_0}^{\vartheta_1} f_{phase}\ \mathrm{d}\vartheta + T_0 \quad (9)$$

is calculated in azimuthal and meridional deflection. The integration of the temperature field follows the requirements of the integration temperature distribution, given by Immohr [10].

The ε variable describes the separation angle, the λ is the wave length of the laser and the f_{phase} is the phase function which contains the derivative:

$$\frac{\partial T(\vartheta,\ \phi)}{\partial\vartheta} = f_{phase} \frac{\Delta\vartheta\ \lambda}{2\ d\ \varepsilon\ c_0}. \quad (10)$$

Here d is the gap width, the $\left(\frac{dn}{dT}\right)^{-1}$ is the modification of the refractive index n in dependency on the temperature T, and the temperature T_0 is used as an initial value for the calculation.

In Figure 5 a work flow for interferogram evaluation of numerical data is shown, namely the forward modelling. The scenario is a heated inner sphere and cooled outer sphere. The integrated temperature field of this case is shown below. The third picture visualizes the variation of the optical path and

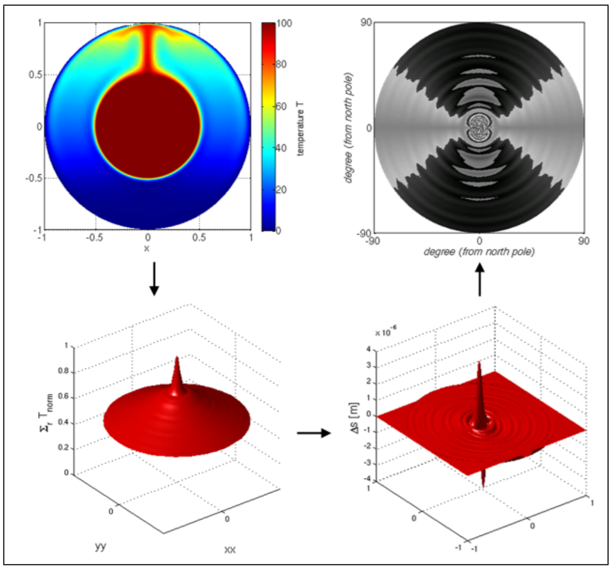

Figure 5: Work flow for interferogram evaluation of numerical data (forward modelling).

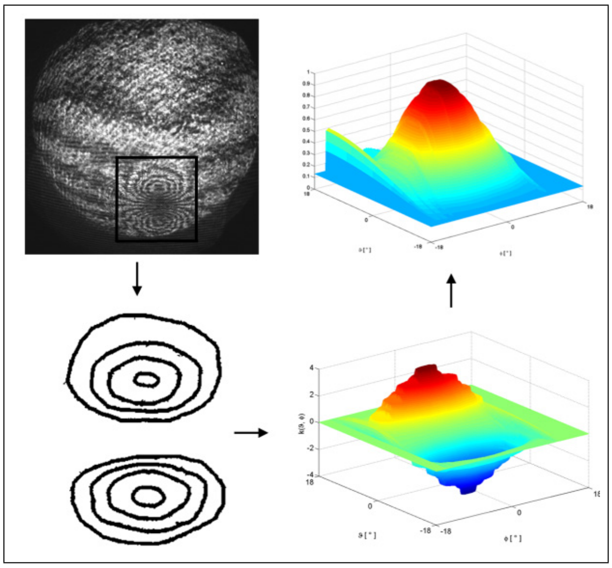

Figure 6: Work flow for interferogram evaluation of experimetal data (inverse modelling).

on upper right side the simulated interferogram from this temperature field is illustrated. These numerical interferogram is for an evaluation for the experimental data.

Figure 6 shows on the top left the measured interferogram with a temperature difference of $\Delta T = 4\ K$, $\Omega = 0\ Hz$ and $V_{rms} = 0\ kV$, as an typical way of image processing. In the image down left, there are the relevant extracted fringes for the flow analysis. There is calculated a phase shift from the extracted fringe pattern for the flow analysis and this is integrated to a temperature field [5]. The right next image shows the phase function of the fringes and on the top right is the temperature field of this phase function demonstrated.

4 Outlook

For further experimental data analysis the challenge is to implement image processing procedure for complex flow structures, concerning of the formation and position of the fringes. Additional, the design of pattern recognition is necessary for an effective comparison and sort of many images and other experimental data with specific criteria.

While the first GeoFlow campaign will probably run, from end of July till November 2008, reflight campaign are under discussion yet, named GeoFlow II. For this is to substitute the fluid with strong temperature dependent fluid to simulate mantle convection. The scientific analyses are comparable to those for GeoFlow I, but the convective behaviour is expected to be quite different to the results by GeoFlow I.

5 Acknowledgement

The GeoFlow project is funded by ESA (grant no. AO-99-049) and by the German Aerospace Center DLR (grant no. 50 WM 0122 and 50 WM 0822). The authors would also like to thank ESA for funding the GeoFlow Topical Team (grant no. 18950/05/NL/VJ). The scientists also thank the industry involved for support, namely Astrium GmbH, Friedrichshafen, Germany and the User Suppoert Center MARS, Naples, Italy and E-USOC, Madrid, Spain.

References

[1] Beltrame, P. ; Travnikov, V. ; Gellert, M. ; Egbers, C.: GEOFLOW: simulation of convection in a spherical shell under central force field. In: *Nonlin. Processes Geophys. 13, pp. 413423* (2006)

[2] Bergemann, K.: *Konvektion im Kugelspalt: Numerische Untersuchung und Bifurkationsanalyse am Beispiel des GeoFlow-Experiments*, University of Potsdam, Diplomarbeit, 2008

[3] Busse, F.H.: Thermal instabilities in rapidly rotating systems. In: *J. Fluid Mech., 44(3), pp. 441-460* (1970)

[4] Carmi, S. ; Joseph, D.D.: Subcritical convective instability. In: *Part II Spherical shells, J. Fluid Mech., 26, pp. 769-778* (1966)

[5] Dahley, N.: *Bildverarbeitung und Strömungsdiagnose für das GeoFlow Experiment Schwerpunkt: Bildauswertung und Ermittlung der Temperaturverteilung*, Brandenburgische Universität Cottbus, Diplomarbeit, 2007

[6] Futterer, B. ; Geller, M. ; Larcher, Th. von ; Egbers, C.: Thermal Convection in rotating spherical shells: an experimental and numerical approach within GeoFlow. In: *Acta Astronautica, pp. 300-307* (2008)

[7] Futterer, B. ; Hollerbach, R. ; Egbers, C.: GeoFlow: 3D numerical simulation of supercritical thermal convective states. In: *15th International Couette Taylor Workshop* (2007)

[8] Hart, J.E. ; Glatzmaier, G.A. ; Toomre, J.: Space-laboratory and numerical simulations of thermal convection in a rotating hemisperical shell with radial gravity. In: *J. Fluid Mech., 173, 26 pp. 519-544* (1986)

[9] Hollerbach, R.: A spectral solution of the magneto-convection equations in spherical geometry. In: *International Journal for Numerical Methods in Fluids 32 pp. 773-797* (2000)

[10] Immohr, J.: *Sphärische Differentialinterferometrie für Raumfahrtanwendungen - Konvektionsströmungen im Kugelspalt unter dem Einfluss axialer und radialer Kraftwirkung*, Universität Bremen, Diss., 2006. – Fortschritt-Bericht VDI Reihe 7, Nr. 481, Düsseldorf

[11] Larcher, Th. von ; Futterer, B. ; Egbers, C. ; Hollerbach, R. ; Chossat, P. ; Beltrame, P. ; Tuckerman, L. ; Feudel, F.: GeoFlow: European Microgravity Experiments on Thermal Convection in Rotating Spherical Shells under influence of Central Force Field. In: *Proceedings of the 3rd International Symposium on Physical Sciences in Space (3rd ISPS 2007)* (2007)

[12] Roberts, P.H.: On the thermal instability of a rotating-fluid sphere containing heat sources. In: *Phil. Trans. Roy Soc. Lon. A, 263, pp. 769-778* (1968)

[13] Travnikov, V. ; Egbers, C. ; Hollerbach, R.: The GeoFlow-experiement on ISS (Part II): numerical simulation. In: *Advances in Space Research 32, pp. 181-189* (2003)